

---

# Learning a High Fidelity Pose Invariant Model for High-resolution Face Frontalization

---

**Jie Cao, Yibo Hu, Hongwen Zhang, Ran He, Zhenan Sun**

National Laboratory of Pattern Recognition, CASIA

Center for Research on Intelligent Perception and Computing, CASIA

Center for Excellence in Brain Science and Intelligence Technology, CAS

University of Chinese Academy of Sciences, Beijing, 100049, China

{jie.cao,yibo.hu,hongwen.zhang}@cripac.ia.ac.cn {rhe,znsun}@nlpr.ia.ac.cn

## Abstract

Face frontalization refers to the process of synthesizing the frontal view of a face from a given profile. Due to self-occlusion and appearance distortion in the wild, it is extremely challenging to recover faithful results and preserve texture details in a high-resolution. This paper proposes a High Fidelity Pose Invariant Model (HF-PIM) to produce photographic and identity-preserving results. HF-PIM frontalizes the profiles through a novel texture fusion warping procedure and leverages a dense correspondence field to bind the 2D and 3D surface space. We decompose the prerequisite of warping into correspondence field estimation and facial texture recovering, which are both well addressed by deep networks. Different from those reconstruction methods relying on 3D data, we also propose Adversarial Residual Dictionary Learning (ARDL) to supervise facial texture map recovering with only monocular images. Exhaustive experiments on both controlled and uncontrolled environments demonstrate that the proposed method not only boosts the performance of pose-invariant face recognition but also dramatically improves high-resolution frontalization appearances.

## 1 Introduction

Face frontalization refers to predicting the frontal view image from a given profile. It is an effective preprocessing method for pose-invariant face recognition as well as other practical systems including face reconstruction and attribute analysis. Due to the appealing prospect in theories and applications, research interest has been lasting for years. In the early stage, most traditional face frontalization methods [7, 13, 14, 8, 39] are 3D-based. These methods mainly leverage theories in monocular face reconstruction to recover 3D faces, and then render frontal view images. The well-known 3D Morphable Model (3DMM) [2] has been widely employed to express facial shape and appearance information. Recently, great breakthroughs have been made by the methods based on generative adversarial networks (GAN) [9]. Those methods frontalize faces from the perspective of 2D image-to-image translation and build deep networks with novel architectures. The visual realism has been improved significantly, for instance, in Multi-PIE [10], some synthesized results [20, 37] from small pose profiles are so photographic that it is difficult for human observers to distinguish them from the real ones. Further, frontalized results have been proved to be effective to tackle the pose discrepancy in face recognition. Through the “recognition via generation” framework, current methods [36, 37] achieve state-of-the-art pose-invariant face recognition performance on multiple datasets including Multi-PIE and IJB-A [23].

Even though much progress has been made, there are still some ongoing issues for in-the-wild face frontalization. For traditional 3D-based approaches, due to the shortage of 3D data and the limited

representation power of backbone 3D model, their performances are commonly less competitive compared with GAN-based methods albeit some improvements [32] have been made. However, GAN-based methods heavily rely on minimizing pixel-wise losses to deal with the noisy data for in the wild settings. As discussed in many other image restoration tasks [19, 21], the consequence is that the outputs lack variations and tend to keep close to the statistical meaning of the training data. The results will be over-smoothed with little high-level texture information. Hence, current frontalization results are less appealing in a high-resolution and the output size is often no larger than  $128 \times 128$ .

To address the above issues, this paper proposes a High Fidelity Pose Invariant Model (HF-PIM) that combines the advantages of 3D and GAN based methods. In HF-PIM, we frontalize the profiles via a novel texture fusion warping procedure. Inspired by recent progress in 3D face analysis, we introduce a dense correspondence field to bind the 2D and 3D surface space. Thus, the prerequisite of our warping procedure is decomposed into two well-constrained problems: correspondence field estimation and facial texture map recovering. We build a deep network to address the two problems and benefit from its greater representation power than traditional 3D based methods. Furthermore, we propose Adversarial Residual Dictionary Learning (ARDL) to get rid of the high reliance on 3D data. Thanks to the 3D-based deep framework and the capacity of ARDL for fine-grained texture representation [5], high-resolution results with faithful texture details can be obtained. We make extensive comparisons with state-of-the-art methods on the IJB-A, LFW [18] and Multi-PIE datasets. We also frontalize  $256 \times 256$  images from CelebA-HQ [22] to push forward the advance in high-resolution face frontalization. Quantitative and qualitative results demonstrate our HF-PIM dramatically improves pose-invariant face recognition and produces photographic high-resolution results potentially benefitting many real-world applications.

To summarize, our main contributions are listed as follows:

- A novel High Fidelity Pose Invariant Model (HF-PIM) is proposed to produce more realistic and identity-preserving frontalized face images with a higher resolution.
- Through dense correspondence field estimation and facial texture map recovering, our warping procedure can frontalize profile images with large poses and preserves abundant latent 3D shape information.
- Without the need of 3D data, we propose ARDL to supervise the process of facial texture map recovering, effectively compensating the texture representation capacity for 3D-based framework.
- A unified end-to-end deep network is built to integrate all algorithmic components, which makes the training process elegant and flexible.
- Extensive experiments on four face frontalization databases demonstrate that HF-PIM not only boosts pose-invariant face recognition in the wild, but also dramatically improves the visual quality of high-resolution images.

## 2 Related Works

In recent years, GAN, proposed by Goodfellow et al. [9], has been successfully introduced into the field of computer vision. GAN can be regarded as a two-player non-cooperative game model. The main components, generator and discriminator, are rivals of each other. The generator tries to map a given input distribution to a target data distribution. Whereas the discriminator tries to distinguish the data produced by the generator from the real one. Due to its remarkable capacity of producing visual realism results, significant improvements have been made in many image generation, translation and completion tasks.

GAN has dominated the field of face frontalization since it is firstly used by DR-GAN [33]. Later, TP-GAN [20] is proposed with a two-pathway structure and perceptual supervision. CAPG-GAN [17] introduce pose guidance through inserting conditional information carried by five-point heatmaps. PIM [37] aims to generate high-quality results through adding regularization items to learn face representations more robust to hard examples. All those methods treat face frontalization as a 2D image-to-image translation problem without considering the intrinsic 3D properties of human face. They indeed perform well in the situation where training data is sufficient and captured well controlled. However, in-the-wild setting often leads to inferior performance, as we discussed in Sec. 1.

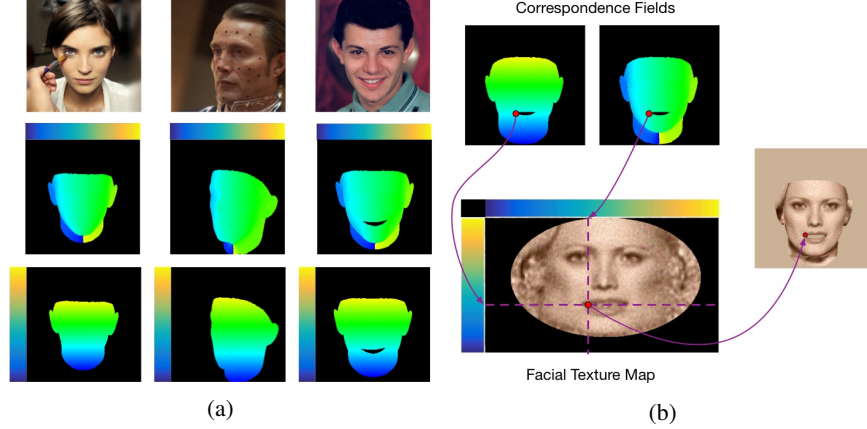


Figure 1: (a) Visual examples of the correspondence field  $F = (u; v)$ . RGB color images are on the first row. Corresponding  $u$  and  $v$  are on the second and the third row respectively. Color indicates the values of the pixels in  $F$ . (b) An visual illustration about the warping procedure proposed in Eq. 1. Those red dots and purple lines indicate the relationships between the facial texture map, correspondence field and the RGB color image.

The attempt to combine prior knowledge of 3D face has been made by FF-GAN [35] and UV-GAN [6]. Their and our methods are all 3D based but there are many differences. In FF-GAN, a CNN is trained jointly to regress the 3DMM coefficients of the input. Those coefficients are integrated as a supplement of low-frequency information. In contrast, we do not employ 3DMM to present shape or texture information. We introduce a novel dense correspondence field and frontalize the profiles through warping. UV-GAN leverages out-of-the-box method for the 2D image to a 3D surface projection. In fact, their network is still a 2D image-to-image translation model (in the facial texture space). In contrast, once the training procedure is finished, our model can estimate the latent 3D information from the profiles without the need of any additional methods. Besides, UV-GAN is proposed as a model for face completion and data augmentation. In this paper, we demonstrate that our method can not only recover faithful frontal view faces but also boost the performance of pose-invariant face recognition.

It is also notable that except face frontalization, there are other ways to eliminate pose discrepancy based on the idea of “recognition via generation”. Inspired by [31], DA-GAN [36], which acts as a 2D face image refiner, is proposed for pose-invariant face recognition. In brief, the refiner improves the quality of data augmented by ordinary methods. The training process benefits from those refined data and the performance is boosted. Thus, DA-GAN is a method for augmenting training data (Note that UV-GAN can be used to benefit face recognition in the same manner with DA-GAN, so it is also a data augmentation method). In contrast, we aim to recover the frontal view from the profile and can be regarded as a data preprocessing method for pose-invariant face recognition. Besides, DA-GAN can be used to augment our training data to bring more improvement.

### 3 High Fidelity Pose Invariant Model

The goal of face frontalization is to model the mapping from profile face  $X$  to corresponding frontal view face  $Y$  ( $X, Y \in \mathbb{R}^{N \times N \times 3}$  and  $\mathbb{R}$  is the RGB color image space). As a reminder, we use  $I_{ij}$  to denote the value of the pixel with coordinate  $(i, j)$  in an image  $I$ . To learn the mapping, image pairs  $(X, \hat{Y})$  are employed for model training, where  $\hat{Y}$  is the ground truth frontal view face. Inspired by recent progress in 3D face analysis [11, 12], we propose a brand-new framework which frontalizes given profile face through recovering geometry and texture information of the 3D face without explicitly building it. Concretely, the facial texture map and a novel correspondence field are leveraged to produce  $Y$  through warping. The facial texture map  $T$  lies in UV space - a space in which the manifold of the face is flattened into a contiguous 2D atlas.  $T$  represents the surface of the 3D face. The correspondence field  $F = (u; v)$  ( $u, v \in \mathbb{R}^{N \times N}$ ) is specified by following statement: assume that the coordinate of a point in  $T$  is  $(u_{ij}, v_{ij})$ , after warping, the corresponding coordinate

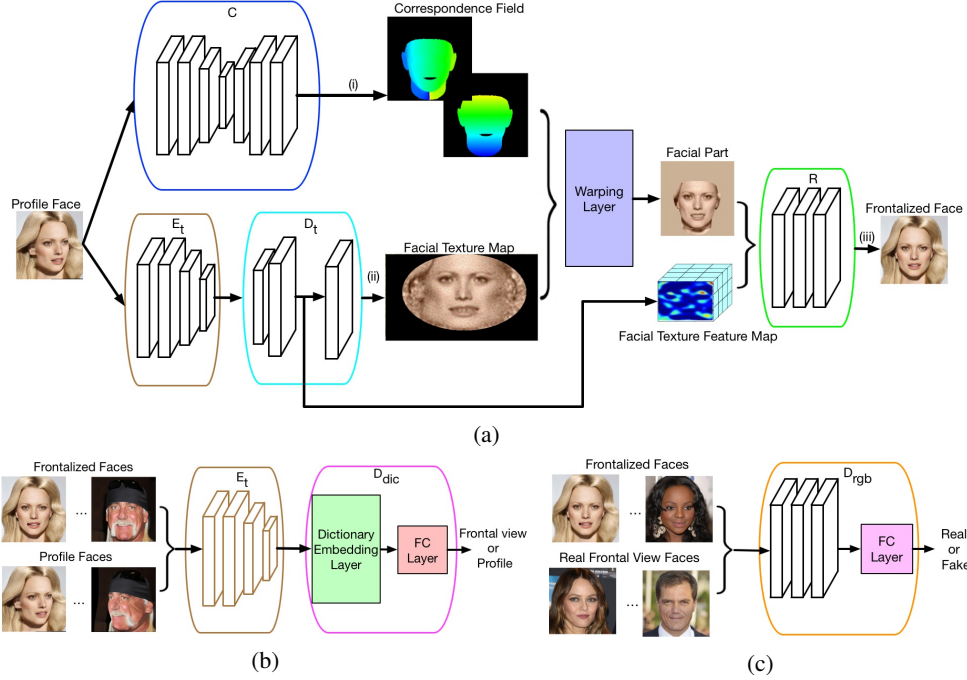


Figure 2: (a) The framework of our HF-PIM to frontalize face images. The procedures of correspondence field estimation (i), facial texture feature map recovering (ii) and frontal view warping (iii) are discussed in Sections 3.1, 3.2 and 3.3, respectively. (b) The discriminator employed for ARDL, which is discussed in Sec. 3.2. “FC Layer” denotes a fully connected layer. (c) The discriminator employed for ordinary adversarial learning, which is discussed in Sec. 3.4.

in  $\mathbf{Y}$  is  $(i, j)$ . Fig. 1 provides an intuitionistic illustration. Formally, given  $\mathbf{T}$  and  $\mathbf{F}$  with respect to  $\mathbf{Y}$ ,  $\mathbf{T}$  is warped into  $\mathbf{Y}$  through the following formulation:

$$Y_{ij} = \text{warp}(i, j; \mathbf{F}, \mathbf{T}) = T_{u_{ij}, v_{ij}} \quad (1)$$

Note that  $\mathbf{T}$  is represented as a bitmap image with a rectangular grid of pixels, i.e.,  $T_{ij}$  is defined if and only if  $i, j \in \mathbb{Z}^+$ . Thus, we employ grid sampling on  $\mathbf{T}$  via a bilinear kernel to determine the value of each pixel in  $\mathbf{Y}$  in our experiment. Our proposed warping procedure inherits the virtue of morphable model construction: geometry and texture are well disentangled whereas bound by dense correspondence. However, there are many limitations for traditional construction methods including highly relying on 3D data, neglect of image background, etc. To overcome those constraints, we design an end-to-end deep neural network to provide  $\mathbf{F}$  and  $\mathbf{T}$  for Eq. 1. The framework is shown in Fig. 2. In the following, we describe how to estimate the correspondence field  $\mathbf{F}$  of the frontal view in Sec. 3.1. Then, the recovering procedure of the facial texture map  $\mathbf{T}$  via ARDL is illustrated in Sec. 3.2. The warping procedure is augmented by fusion warping in Sec. 3.3. Regularization items and the overall loss function are introduced in Sec. 3.4.

### 3.1 Correspondence Field Estimation

To obtain the ground truth correspondence field  $\hat{\mathbf{F}}$  of monocular frontal view face images for training, we employ face reconstruction method for 3D shape information estimation. Concretely, we employ BFM [28] as the 3D face model. Through the model fitting method proposed by [40], we get estimated shape parameters containing coordinates of vertices. To build  $\hat{\mathbf{F}}$ , we map those vertices to UV space via the cylindrical unwrapping described in [3]. Those non-visible vertices are culled via z-buffering.

To infer the correspondence field of the frontal view from the profile image, we build a transformative autoencoder,  $C$ , with U-Net architecture. Given the input,  $C$  first encodes it into pose-invariant shape representations and then recover correspondence field of frontal view. Further, those shortcuts in

U-Net guarantee the preservation of spatial information in the output. To supervise  $C$  during training, we minimize the pixel-wise error between the estimated map and the ground truth  $\hat{\mathbf{F}}$ , namely:

$$L_{corr} = \left\| C(\mathbf{X}) - \hat{\mathbf{F}} \right\|_1 \quad (2)$$

where  $\|\cdot\|_1$  denotes calculating the mean of the element-wise absolute value summation of a matrix.

### 3.2 Facial Texture Map Recovery

We employ a transformative autoencoder consisting of the encoder  $E_t$  and the decoder  $D_t$  for facial texture map recovering. However, the ground truth facial texture map  $\hat{\mathbf{T}}$  of monocular face image captured in the wild is absent. To sidestep the demand for  $\hat{\mathbf{T}}$ , we introduce Adversarial Residual Dictionary Learning (ARDL) which provides supervision for learning. During the training procedure, only  $\hat{\mathbf{Y}}$  is required instead of  $\hat{\mathbf{T}}$ .

The learning dictionary is set as: given a set of texture feature embeddings  $\mathbf{B} = \{\mathbf{b}_1, \dots, \mathbf{b}_n\}$  and a learnable codebook  $\mathbf{C} = \{\mathbf{c}_1, \dots, \mathbf{c}_m\}$  containing  $m$  codewords with  $d$  dimensional, the corresponding residual vector is denoted as  $\mathbf{r}_{ik} = \mathbf{b}_i - \mathbf{c}_k$ , for  $i = 1, \dots, n$  and  $k = 1, \dots, m$ . Through dictionary encoding, a fixed length representation  $\mathbf{E} = \{\mathbf{e}_1, \dots, \mathbf{e}_m\}$  can be calculated as follows:

$$\mathbf{e}_k = \sum_{i=1}^n \mathbf{e}_{ik} = \sum_{i=1}^n w_{ik} \mathbf{r}_{ik} \quad (3)$$

where  $w_{ik}$  is the corresponding weight for  $\mathbf{r}_{ik}$ . Inspired by [34] that assigns a descriptor to each codeword, we make those weights learnable. Concretely, the assigning weight is given by:

$$w_{ik} = \frac{\exp(-s_k \|\mathbf{r}_{ik}\|^2)}{\sum_{j=1}^m \exp(-s_j \|\mathbf{r}_{ij}\|^2)} \quad (4)$$

where  $\mathbf{s} = (s_1, \dots, s_m)$  is the smoothing factor, which is also learnable. We denote the mapping from feature embeddings to dictionary representation as  $D_{dic}$ . The encoder  $E_t$  is also employed to extract features for the dictionary learning.

We combine dictionary representation with adversarial learning, i.e., propose ARDL based on such an observation: when the identity label is fixed, for  $\mathbf{X}$  across different poses, the recovered texture map  $\mathbf{T}$  should be invariant. To this end,  $E_t$  should eliminate those discrepancies caused by different views and encode the input into pose-invariant facial texture representation. We introduce adversarial learning mechanism to supervise  $E_t$  by making  $D_{dic}$  as its rival. Formally, the adversarial loss introduced by ARDL is formulated as:

$$L_{adv} = \mathbb{E}_{\mathbf{X} \sim p_{data}} [\log D_{dic}(E_t(\mathbf{X}))] \quad (5)$$

accordingly,  $D_{dic}$  is optimized to minimize:

$$L_{dic} = \mathbb{E}_{\mathbf{X}, \hat{\mathbf{Y}} \sim p_{data}} [\log D_{dic}(E_t(\hat{\mathbf{Y}})) + \log(1 - D_{dic}(E_t(\mathbf{X})))] \quad (6)$$

where we add a fully connected (FC) layer upon  $D_{dic}$  to make binary predictions standing for real and fake. Through optimizing Eq. 5 and 6 alternatively,  $E_t$  manages to make the encodings of the profile and the frontal view as similar as possible, i.e., learn to represent the facial texture map even from the profile. In the meantime,  $D_{dic}$  tries to find the clues standing for pose information, which provides the adversarial supervision information for  $E_t$ .

### 3.3 Fusion Warping

In this subsection, we propose fusion warping that augments the procedure in Eq. 1 to produce the non-facial parts simultaneously with producing facial one. As indicated by Fig. 1b, ordinary warping only produces the facial part of the image. The values of pixels standing for non-facial parts are undefined, so post process is necessary to complete the missing regions. In our fusion warping, a fully connected network  $R$  is employed to integrate the warping result with the second last convolution layers in  $D$ . The final output of  $D$ , namely the predicted facial texture map, remains to be warped into the facial region through Eq. 1. In the meantime, the output of the second last layer within  $D$ , which can be regarded as the facial texture feature map (denoted as  $T^*$ ), is fed into  $R$  along with the warped facial part. The reconstruction loss is introduced by  $R$  as follows:

$$L_{rec} = \left\| R(\text{warp}(\mathbf{F}, \mathbf{T}) \odot \mathbf{T}^*) - \hat{\mathbf{Y}} \right\|_1 \quad (7)$$

where  $\odot$  denotes the concatenation operation on the feature channel. Through optimizing Eq. 7,  $R$  is trained to add the background through the information provided by  $\mathbf{T}^*$  as well as keep the visual realism and consistency with  $\mathbf{X}$ .

### 3.4 Overall Training Method

Following previous work [21, 20], we also add the perceptual loss to integrate domain knowledge of identities. An identity preserving network, e.g., VGG-Face [26] or Light CNN [15], can be employed to supervise the frontalized results to be as close to the ground truth as possible in feature-level. Formally, the perceptual loss is formulated as:

$$L_p = \left\| \phi(R(\text{warp}(\mathbf{F}, \mathbf{T}) \odot \mathbf{T}^*)) - \phi(\hat{\mathbf{Y}}) \right\|_2^2 \quad (8)$$

where  $\phi(\cdot)$  denotes the extracted identity representation obtained by the second last fully connected layer within the identity preserving network and  $\|\cdot\|_2$  denotes the vector 2-norm.

We also introduce the adversarial loss in the RGB color image space following those GAN-based methods [33, 20, 17, 37, 35]. A CNN named  $D_{rgb}$  is employed to give adversarial supervision in color space. Note that our method can be easily extended to those advanced versions [1, 25] of GAN. As it is not our contribution, we simply use the original version [9] and find it already produce a good performance.

In summary, all the involved algorithmic components in our network are differentiable. Hence, the parameters can be optimized in an end-to-end manner via gradient backpropagation. The whole training process is described in Algorithm 1.

## 4 Experiments

### 4.1 Experimental Settings

**Datasets.** Four datasets are involved in our experiments: Multi-PIE [10], LFW [18], IJB-A [23], and CelebA-HQ [22]. Multi-PIE is established for studying on PIE (pose, illumination and expression) invariant face recognition. 20 illumination conditions, 13 poses within 90 yaw angles and 6 expressions of 337 subjects were captured in controlled environments. LFW is a benchmark database for face recognition. Over 13,000 face images are captured in unconstrained environments. IJB-A is the most challenging unconstrained face recognition dataset at present. It has 5, 396 images and 20, 412 video frames of 500 subjects with large pose variations. CelebA [24] is a large-scale face attributes dataset. Contained images cover large pose variations and background clutter. CelebA-HQ is a high-resolution subset established by [22]. Since Multi-PIE, LFW and IJB-A consist of images with relatively low resolutions, we use CelebA-HQ for high-resolution ( $256 \times 256$ ) face frontalization.

**Implementation Details.** The training set is drawn from Multi-PIE and CelebA-HQ. We follow the protocol in [33] to split the Multi-PIE dataset. The first 200 subjects are used for training and the rest 137 ones for testing. Each testing identity has one gallery image from his/her first appearance. Hence, there are 72,000 and 137 images in the probe and gallery sets, respectively. For CelebA-HQ, we

---

**Algorithm 1** Training algorithm of HF-PIM

---

```
1: Input: profile  $\mathbf{X}$ , the ground truth frontal view  $\hat{\mathbf{Y}}$  with ground truth correspondence field  $\hat{\mathbf{F}}$ ,  
   maximum iteration  $iter$  and the identity preserving network [15].  
2: Output: the frontalized result  $\mathbf{Y}$   
3: Initializing  $C, E_t, D_t, R, D_{dic}, D_{rgb}$   
4:  $i \leftarrow 0$   
5: while  $i < iter$  do  
6:   Sampling training data  
7:   Model forward propagation  
8:   Calculating  $L_{rec}, L_{corr}, L_{dic}, L_{adv}$  and  $L_p$   
9:   Calculating the adversarial losses in the RGB color image space, i.e.,  $L_g$  (for the generator)  
   and  $L_d$  (for the discriminator)  
10:   $L \leftarrow L_{rec} + L_{corr} + L_{adv} + L_p + L_g$   
11:  Optimize  $C, R, E_t, D_t$  by minimizing  $L$   
12:  Optimize  $D_{dic}$  by minimizing  $L_{dic}$   
13:  Optimize  $D_{rgb}$  by minimizing  $L_d$   
14:   $i \leftarrow i + 1$   
15: end while
```

---

Table 1: Comparisons on rank-1 recognition rates (%) across views under Multi-PIE Setting 2.

Method	$\pm 15^\circ$	$\pm 30^\circ$	$\pm 45^\circ$	$\pm 60^\circ$	$\pm 75^\circ$	$\pm 90^\circ$
DR-GAN [33]	94.9	91.1	87.2	84.6	-	-
FF-GAN [35]	94.6	92.5	89.7	85.2	77.2	61.2
TP-GAN [20]	98.7	98.1	95.4	87.7	77.4	64.6
CAPG-GAN [17]	99.8	99.6	97.3	90.3	83.1	66.1
PIM [37]	99.3	99.0	98.5	98.1	95.0	86.5
<b>HF-PIM(Ours)</b>	<b>99.99</b>	<b>99.98</b>	<b>99.88</b>	<b>99.14</b>	<b>96.40</b>	<b>92.32</b>

apply head pose estimation [40] to find those frontal view faces and employ them (19, 203 images) for training. We choose those images with large poses (5, 998 ones) for testing. Apparently, there are no overlap between our training and testing sets. LFW and IJB-A are only used for testing. Note that the images selected for training in CelebA-HQ are all frontal view, and we employ the face profiling method in [39] to make corresponding profiles. We adapt the model architecture in [38] to build our networks. We use Adam optimizer with a learning rate of  $1e-4$  and  $\beta_1 = 0.5, \beta_2 = 0.99$ . Our proposed method is implemented based on the deep learning library Pytorch [27]. Two NVIDIA Titan X GPUs with 12GB GDDR5X RAM is employed for the training and testing process. Please refer to supplementary material Sec. A for network architectures and Sec. B for full details on training pairs generation.

**Evaluation Metrics.** For ordinary image generation tasks, the Inception Score (IS) [30] has been employed wildly to measure the performance. Note that IS can be only computed on close-set classification tasks, so it cannot be applied to measure generation model specified for face frontalization (which is an open-set problem). Recently, a more principled and comprehensive metric, the Fréchet Inception Distance (FID) [16], has been proposed to replace IS. For most face frontalization methods, they measure the performance by “recognition via generation”, which basically can be interpreted as leveraging a modification of FID to measure the face recognition rate. “Recognition via generation” means profiles are frontalized first, and then the recognition performance is evaluated on those processed face images. This procedure has been discussed in detail in previous methods [33, 20, 35]. In this paper, we follow those methods to measure the performance quantificationally and make it possible to compare our results with them. Besides, visual inception is also compared, as most GAN-based methods do.

## 4.2 Frontalization Results in Controlled Situations

In this subsection, we systematically compare our method with DR-GAN[33], TP-GAN[20], FF-GAN [35], PGCA-GAN [17] and PIM [37] on the Multi-PIE dataset. Those profiles with extreme poses

Table 2: Face recognition performance (%) comparisons for in-the-wild datasets. The left part is compared on LFW and the right side is on IJB-A. The results on IJB-A are averaged over 10 testing splits. “-” means the result is not reported.

Method	LFW		Method	IJB-A			
	Verification			Verification		Recognition	
	ACC	AUC		FAR=0.01	FAR=0.001	Rank-1	Rank-5
LFW-3D [14]	93.62	88.36	DR-GAN [33]	77.4±2.7	53.9±4.3	85.5±1.5	94.7±1.1
Ferrari [8]	-	94.29	VGG-Face [26]	80.5±3.0	-	91.3±1.1	-
LFW-HPEN [39]	96.25	99.39	FF-GAN [35]	85.2±1.0	66.3±3.3	90.2±0.6	95.4±0.5
FF-GAN [35]	96.42	99.45	LightCNN [15]	91.5±1.0	84.3±2.4	93.0±1.0	-
CAPG-GAN [17]	99.37	99.90	PIM [37]	93.3±1.1	87.5±1.8	94.4±1.1	-
HF-PIM(Ours)	<b>99.41</b>	<b>99.92</b>	HF-PIM(Ours)	<b>95.2±0.7</b>	<b>89.7±1.4</b>	<b>96.1±0.5</b>	<b>97.9±0.2</b>



Figure 3: Visual comparisons of face frontalization results. The samples on the left are drawn from LFW and the right side are from IJB-A.

(75° and 90°) are very challenging cases. Our performances are tested following the protocol of the setting 2 provided by Multi-PIE. We use the frontalized faces for verification and employ the face recognizer [15] used by [37]. The results are reported across different poses in Table 1. For those poses less than 60°, the performances of most methods are quite good whereas our method performs better. We infer that the performance has almost saturated in this case. For those extreme poses, our methods can still produce visually convincing results and achieve state-of-the-art recognition performance. Please refer to supplementary material Sec. C for visual inspections. In general, when testing on Multi-PIE, due to its balanced data distribution and highly controlled environment, most methods perform relatively well (except those extreme poses).

### 4.3 Frontalization Results in the Wild

Extending face frontalization to in-the-wild setting is a very challenging problem with significant importance. We focus on testing on IJB-A and LFW in this subsection. Following FF-GAN [35] and CAPG-GAN [17], we evaluate face verification performance on the frontalized results of the 6000 face pairs provided by LFW. For IJB-A, both verification and identification are tested in 10-fold cross-validation. The results are summarized in Table 2. All the methods are tested with the same setting. Note that the training set of IJB-A is not been used by any involved method for comparison.

Through quantitative comparisons, our method shows a significant improvement for pose-invariant face verification and recognition. The visual comparison<sup>1</sup>, which is shown in Fig 3, also proves our superiority of preserving identity information and texture details. Thanks to the 3D-based framework and powerful adversarial residual dictionary learning, our HF-PIM produces results with very high fidelity. For other methods, they indeed produce reasonable images but redundant manipulations can be observed. For instance, DR-GAN make the eyes of the subject in the middle in IJB-A open; TP-

<sup>1</sup>Visual results produced by other methods are released by their authors. Different methods usually report visual examples of different identities. We try our best to find those identities reported by most methods.





Figure 4: High-resolution frontalized results on the testing set of CelebA-HQ. The first row is the input profile images. The second row is the frontalized images produce by our HF-PIM. The results of CAPG-GAN (on the left for each subject) and TP-GAN (on the right) are shown in the third row.

GAN and CAPR-GAN tend to change the skin color and background. Please refer to supplementary material Sec. D for more frontalized examples.

#### 4.4 High-Resolution Face Frontalization

Generating high-resolution results has great importance on extending the application of face frontalization. However, due to its difficulty, few methods consider producing images with size larger than  $128 \times 128$ . To further demonstrate our superiority, frontalized  $256 \times 256$  results on CelebA-HQ are proposed in this paper. Some samples are shown in Fig 4. We also make comparisons with TP-GAN and CAPG-GAN. Note that since results on CelebA-HQ have not been reported by previous methods, we contact the authors to get their model and produce  $128 \times 128$  results through carefully following their instructions. The images in CelebA-HQ contain rich textures that are difficult for the generator to reproduce faithfully. Even in such a challenging situation, HF-PIM is still able to produce plausible results. The results of [17] and [20] look less appealing. Due to limitations of space, most visual results are shown in supplementary material Sec. E.

Existing methods [20, 33, 37, 35, 17] measure the performance of face recognition to reflect the quality of frontalized results. This measurement cannot be applied to those datasets without identity labels (like CelebA-HQ) and neglects texture information that are not sensitive to identity. However, the neglected textures also play an import role on the visual quality and should be preserved faithfully. For face attribute analysis, data augmentation and many other practical applications, recovering high-resolution frontal view with detailed texture information has great potential for making progress. Finding new applications for face frontalization and putting forward new metrics need further research.

## 5 Ablation Study and other Visual Results

The superiority of our novel 3D based deep framework has been verified by the comparisons with other methods. However, one could be interested in the effect of ARDL. In this section, we compare our HF-PIM with several variations to demonstrate its effectiveness. Specifically, we investigate following conditions:

Table 3: Face recognition performance (%) comparisons for our HF-PIM and its variations on the IJB-A dataset. The results on IJB-A are averaged over 10 testing splits.

	Verification		Recognition	
	FAR=0.01	FAR=0.001	Rank-1	Rank-5
HF-PIM	95.3±0.7	89.9±1.3	96.4±0.5	98.1±0.2
Variation(a)	95.0±0.7	89.1±1.5	95.6±0.8	97.0±0.4
Variation(b)	94.7±0.8	89.1±1.6	95.2±0.9	96.9±0.4
Variation(c)	94.1±1.0	87.7±1.9	94.3±1.1	96.1±0.8



Figure 5: Qualitative comparisons on synthesis results between HF-PIM and its variants. From top to down, those rows are the input, frontalized results produced by HF-PIM, variation (a), (b) and (c), respectively.

- (a) The dictionary learning is removed from ARDL. In this case, the dictionary embedding layer is replaced by a fully connected layer.
- (b) The adversarial learning is removed from ADLR. In this case,  $D_{dic}$  is removed and  $L_{adv}$  is obtained through calculating the vector 2-norm of  $(E_t(\hat{Y}) - E_t(X))$ .
- (c) ARDL is directly removed. In this case,  $D_{dic}$  is removed and  $L_{adv}$  is excluded from the training process.

The quantitative comparisons on IJB-A are reported in Table. 3. Visual examples drawn from the testing set of CelebA-HQ are shown in Fig. 5. Note that we add the pixel-wise loss on the warped face for all those models for comparison. So, the HF-PIM here is slightly different from the original version. The main purpose is to make the warped face more visually appealing. Those warped faces,





Figure 6: Visualization of intermediate results produced by our HF-PIM. For each identity, the images in the first row are the frontalized results and the facial part, the image in the second row is the facial texture map and images in the second row are the dense correspondence field.

facial texture maps produced by HF-PIM are shown in Fig. 6 for anyone who is interested. From Table. 3 and Fig. 5, we can observe that: (1) Different settings on facial texture map recovering influence both visual quality and recognition performance, and the two indices are basically consistent with each other. (2) The supervision on the facial texture recovery process is very important. So, most obvious artifacts can be observed on Variation (c). (3) Both adversarial learning and dictionary embedding improve the performance, and the best performance is obtained when they work together. The contribution of adversarial learning is more significant.

## 6 Conclusion

This paper has proposed HF-PIM to produce realistic and identity-preserving frontalization results with a higher resolution. HF-PIM combines the advantages of 3D and GAN based methods and frontalizes profile images via a novel facial texture fusion warping procedure. Through leveraging a novel dense correspondence field, the prerequisite of warping is decomposed into correspondence field estimation and facial texture recovering, which are well addressed by a unified end-to-end deep network. We also have introduced Adversarial Residual Dictionary Learning to supervise

facial texture map recovering without the need of 3D data. Exhaustive experiments have shown proposed method can preserve more identity information as well as texture details, which make the high-resolution results far more realistic.

## References

- [1] Arjovsky, Martin, Chintala, Soumith, and Bottou, Léon. Wasserstein GAN. In *ICML*, 2017.
- [2] Blanz, Volker and Vetter, Thomas. A morphable model for the synthesis of 3D faces. In *SIGGRAPH*, 1999.
- [3] Booth, James and Zafeiriou, Stefanos. Optimal UV spaces for facial morphable model construction. In *ICIP*, 2014.
- [4] Bulat, Adrian and Tzimiropoulos, Georgios. How far are we from solving the 2D & 3D face alignment problem?(and a dataset of 230,000 3D facial landmarks). In *ICCV*, 2017.
- [5] Dana, Han Zhang Jia Xue Kristin. Deep TEN: Texture encoding network. In *CVPR*, 2017.
- [6] Deng, Jiankang, Cheng, Shiyang, Xue, Niannan, Zhou, Yuxiang, and Zafeiriou, Stefanos. UV-GAN: Adversarial facial UV map completion for pose-invariant face recognition. In *CVPR*, 2018.
- [7] Dovgand, Roman and Basri, Ronen. Statistical symmetric shape from shading for 3D structure recovery of faces. In *ECCV*, 2004.
- [8] Ferrari, Claudio, Lisanti, Giuseppe, Berretti, Stefano, and Del Bimbo, Alberto. Effective 3D based frontalization for unconstrained face recognition. In *ICPR*, 2016.
- [9] Goodfellow, Ian, Pouget-Abadie, Jean, Mirza, Mehdi, Xu, Bing, Warde-Farley, David, Ozair, Sherjil, Courville, Aaron, and Bengio, Yoshua. Generative adversarial nets. In *NIPS*, 2014.
- [10] Gross, Ralph, Matthews, Iain, Cohn, Jeffrey, Kanade, Takeo, and Baker, Simon. Multi-PIE. *IVC*, 2010.
- [11] Güler, Rıza Alp, Trigeorgis, George, Antonakos, Epameinondas, Snape, Patrick, Zafeiriou, Stefanos, and Kokkinos, Iasonas. Densereg: Fully convolutional dense shape regression in-the-wild. In *CVPR*, 2017.
- [12] Güler, Rıza Alp, Neverova, Natalia, and Kokkinos, Iasonas. DensePose: Dense human pose estimation in the wild. In *CVPR*, 2018.
- [13] Hassner, Tal. Viewing real-world faces in 3D. In *ICCV*, 2013.
- [14] Hassner, Tal, Harel, Shai, Paz, Eran, and Enbar, Roee. Effective face frontalization in unconstrained images. In *CVPR*, 2015.
- [15] He, Ran, Wu, Xiang, Sun, Zhenan, and Tan, Tieniu. Learning invariant deep representation for NIR-VIS face recognition. In *AAAI*, 2017.
- [16] Heusel, Martin, Ramsauer, Hubert, Unterthiner, Thomas, Nessler, Bernhard, Klambauer, Günter, and Hochreiter, Sepp. GANs trained by a two time-scale update rule converge to a Nash equilibrium. In *NIPS*, 2017.
- [17] Hu, Yibo, Wu, Xiang, Yu, Bing, He, Ran, and Sun, Zhenan. Pose-guided photorealistic face rotation. In *CVPR*, 2018.
- [18] Huang, Gary B, Ramesh, Manu, Berg, Tamara, and Learned-Miller, Erik. Labeled faces in the wild: A database for studying face recognition in unconstrained environments. Technical report, University of Massachusetts, Amherst, 2007.
- [19] Huang, Huaibo, He, Ran, Sun, Zhenan, and Tan, Tieniu. Wavelet-SRnet: A wavelet-based CNN for multi-scale face super resolution. In *ICCV*, 2017.

- [20] Huang, Rui, Zhang, Shu, Li, Tianyu, and He, Ran. Beyond face rotation: Global and local perception GAN for photorealistic and identity preserving frontal view synthesis. In *ICCV*, 2017.
- [21] Johnson, Justin, Alahi, Alexandre, and Fei-Fei, Li. Perceptual losses for real-time style transfer and super-resolution. In *ECCV*, 2016.
- [22] Karras, Tero, Aila, Timo, Laine, Samuli, and Lehtinen, Jaakko. Progressive growing of GANs for improved quality, stability, and variation. In *ICLR*, 2018.
- [23] Klare, Brendan F., Jain, Anil K., Klein, Ben, Taborsky, Emma, Blanton, Austin, Cheney, Jordan, Allen, Kristen, Grother, Patrick, Mah, Alan, and Burge, Mark. Pushing the frontiers of unconstrained face detection and recognition: IARPA Janus Benchmark A. 2015.
- [24] Liu, Ziwei, Luo, Ping, Wang, Xiaogang, and Tang, Xiaoou. Deep learning face attributes in the wild. In *ICCV*, 2015.
- [25] Mao, Xudong, Li, Qing, Xie, Haoran, Lau, Raymond YK, Wang, Zhen, and Smolley, Stephen Paul. Least squares generative adversarial networks. In *ICCV*, 2017.
- [26] Parkhi, Omkar M, Vedaldi, Andrea, Zisserman, Andrew, et al. Deep face recognition. In *BMVC*, 2015.
- [27] Paszke, Adam, Gross, Sam, Chintala, Soumith, Chanan, Gregory, Yang, Edward, DeVito, Zachary, Lin, Zeming, Desmaison, Alban, Antiga, Luca, and Lerer, Adam. Automatic differentiation in pytorch. In *NIPS-W*, 2017.
- [28] Paysan, Pascal, Knothe, Reinhard, Amberg, Brian, Romdhani, Sami, and Vetter, Thomas. A 3D face model for pose and illumination invariant face recognition. In *AVSS*, 2009.
- [29] Romdhani, Sami and Vetter, Thomas. Estimating 3D shape and texture using pixel intensity, edges, specular highlights, texture constraints and a prior. In *CVPR*, 2005.
- [30] Salimans, Tim, Goodfellow, Ian, Zaremba, Wojciech, Cheung, Vicki, Radford, Alec, and Chen, Xi. Improved techniques for training GANs. In *NIPS*, 2016.
- [31] Shrivastava, Ashish, Pfister, Tomas, Tuzel, Oncel, Susskind, Josh, Wang, Wenda, and Webb, Russ. Learning from simulated and unsupervised images through adversarial training. In *CVPR*, 2017.
- [32] Tran, Luan and Liu, Xiaoming. Nonlinear 3D face morphable model. In *CVPR*, 2018.
- [33] Tran, Luan, Yin, Xi, and Liu, Xiaoming. Disentangled representation learning GAN for pose-invariant face recognition. In *CVPR*, 2017.
- [34] Van Gemert, Jan C, Geusebroek, Jan-Mark, Veenman, Cor J, and Smeulders, Arnold WM. Kernel codebooks for scene categorization. In *ECCV*, 2008.
- [35] Yin, Xi, Yu, Xiang, Sohn, Kihyuk, Liu, Xiaoming, and Chandraker, Manmohan. Towards large-pose face frontalization in the wild. In *ICCV*, 2017.
- [36] Zhao, Jian, Xiong, Lin, Jayashree, Panasonic Karlekar, Li, Jianshu, Zhao, Fang, Wang, Zhecan, Pranata, Panasonic Sugiri, Shen, Panasonic Shengmei, Yan, Shuicheng, and Feng, Jiashi. Dual-agent GANs for photorealistic and identity preserving profile face synthesis. In *NIPS*, 2017.
- [37] Zhao, Jian, Cheng, Yu, Xu, Yan, Xiong, Lin, Li, Jianshu, Zhao, Fang, Jayashree, Karlekar, Pranata, Sugiri, Shen, Shengmei, Xing, Junliang, et al. Towards pose invariant face recognition in the wild. In *CVPR*, 2018.
- [38] Zhu, Jun-Yan, Park, Taesung, Isola, Phillip, and Efros, Alexei A. Unpaired image-to-image translation using cycle-consistent adversarial networks. In *ICCV*, 2017.
- [39] Zhu, Xiangyu, Lei, Zhen, Yan, Junjie, Yi, Dong, and Li, Stan Z. High-fidelity pose and expression normalization for face recognition in the wild. In *CVPR*, 2015.
- [40] Zhu, Xiangyu, Lei, Zhen, Liu, Xiaoming, Shi, Hailin, and Li, Stan Z. Face alignment across large poses: A 3D solution. In *CVPR*, 2016.

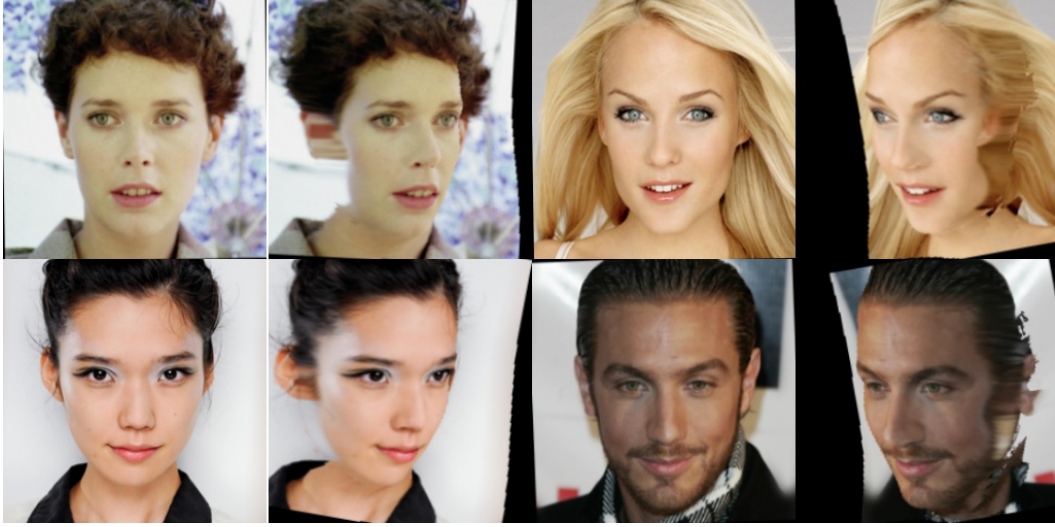


Figure 7: Examples of training data pairs. Those profiles are synthesized by other methods.

## A. Implementation Details

**Network Architecture.** We adapt our network architectures from [38]. Below, we follow the naming convention of [19], Let  $c7s1 - k$  denote a  $7 \times 7$  Convolution-BatchNorm- ReLU layer with  $k$  filters and stride 1.  $dk$  denotes a  $3 \times 3$  Convolution-BatchNorm-ReLU layer with  $k$  filters, and stride 2. Reflection padding was used to reduce artifacts.  $Rk$  denotes a residual block that contains two  $3 \times 3$  convolutional layers with the same number of filters on both layer.  $uk$  denotes a  $3 \times 3$  fractional-strided-Convolution- BatchNorm-ReLU layer with  $k$  filters, and stride  $\frac{1}{2}$ .

The encoder of  $C$  consists of:

$$c7s1 - 32, d64, d128, R128 \times 6, u64, u32, c7s1 - 64$$

$E_t$  consists of:

$$c7s1 - 32, d64, d128, R128 \times 6, u64, u32, c7s1 - 3$$

Corresponding decoders have mirror structures of the encoders.

Our  $R$  consists of:

$$c7s1 - 32, d64, d128, u64, u32, c7s1 - 3$$

**Weights for Different Losses.** The weight of  $L_{rec}$  is assigned to 1. All the other weights are assigned to 0.1. We do not take much time on trying different weights and find this setting already produces very good results.

## B. Face Profiling Method for Making Training Data Pairs

For the Multi-PIE dataset, subjects have images across different poses captured simultaneously. Those images are perfect for training. But images in CelebA-HQ are all captured in the wild. So, for the images in training set from CelebA-HQ, we first detect the landmarks through the method in [4]. We fit the 3DMM provide by [28] through the Multi-Features Framework [29] to get the estimated 3D shape information. Through 3D shape information, we rotate those images by employing the method in [40]. Some samples profiled in this procedure are shown in 7. Note that [40] has limited capacity for face frontalization because they cannot infer those missing texture. During training, we feed those profiles to our model as the input, and the frontal view images are used as the ground truth.

### C. Visual Results on Multi-PIE

Frontalized examples on Multi-PIE are shown in Figures 8, 9, 10 and 11. For each subject, the input image is on the top, the frontalized result is in the middle and the ground truth for reference is on the bottom. The ID numbers in those figures are consecutive (from 201 to 300). We can see that for most subjects both the frontalized results preserve both the visual realism and the characteristics of identities very well. However, for instance, the results of subject 259 and 260 may look less convincing. We infer that it is caused by the unbalanced data distribution in race during the training procedure.

### D. Additional Visual Results on IJB-A

More frontalized examples on IJB-A are shown in Fig. 12. The first and the third rows are the input images. The second and the fourth rows are corresponding frontalized images. Note that profile faces from in-the-wild dataset like IJB-A have no available frontal view images as ground truth. We can see that for this challenging in-the-wild condition, the characteristics of identities are still well preserved by our HF-PIM.

### E. Additional Visual Results on CelebA-HQ

For high-resolution frontalization, the flaws in texture recovery will be exaggerated. Besides, in-the-wild setting brings significant variations in pose, illumination and expression. Thus, face frontalization in CelebA-HQ is an extremely challenging task. We are the first to study on this case and obtain fairly visual appealing results, as shown in Fig. 13 and 14. For each subject, the input image is on the upper row and the frontalized result is on the lower row. In the future, we will focus on generating higher-resolution (like  $512 \times 512$ ) and more realistic results.





Figure 8: Visual results on Multi-PIE. The numbers stand for the ID numbers of the subjects below. For each subject, the input image is on the top, the frontalized result is in the middle and the ground truth on the bottom.



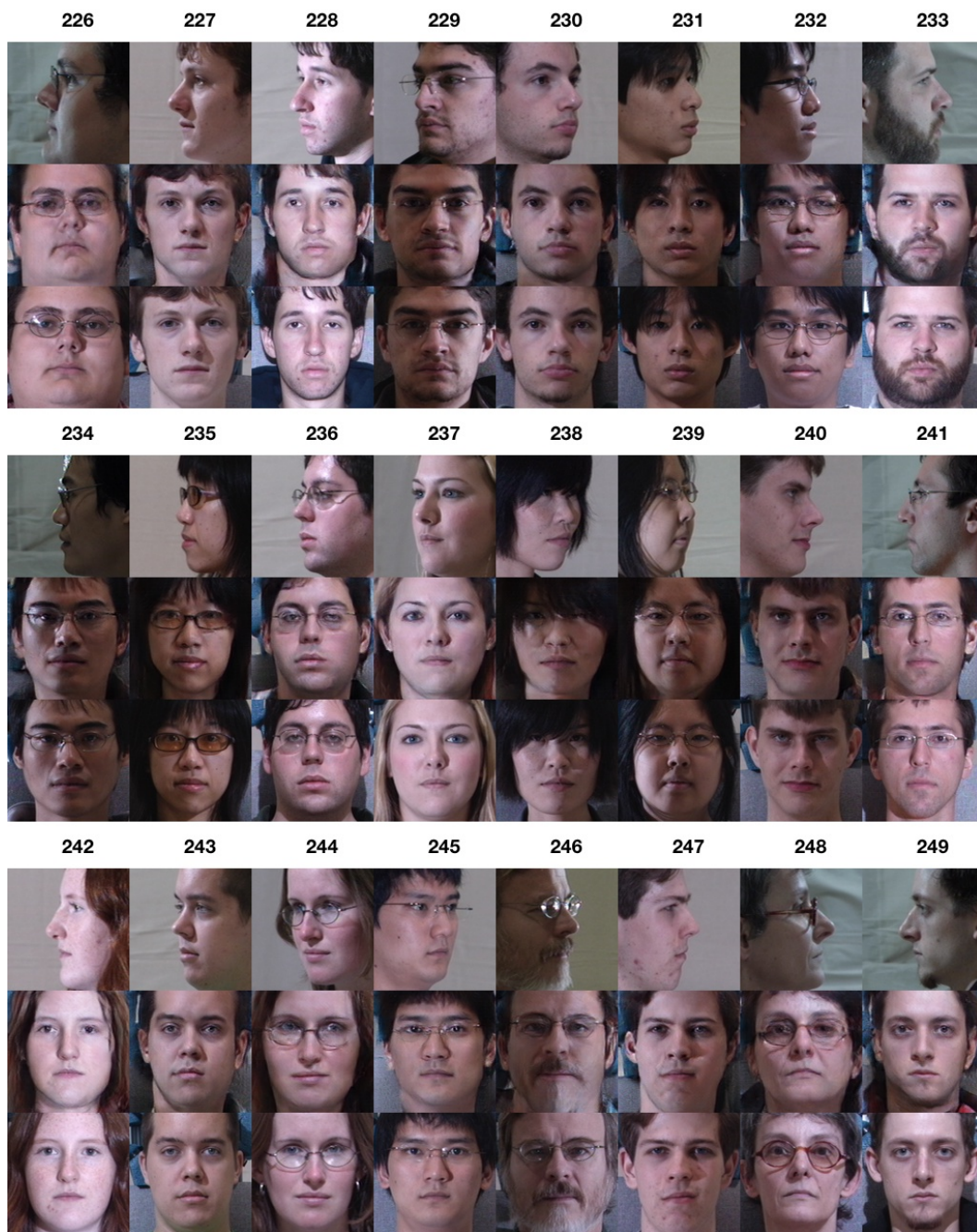


Figure 9: More visual results on Multi-PIE.



Figure 10: More visual results on Multi-PIE.





Figure 11: More visual results on Multi-PIE.



Figure 12: More results on IJB-A.





Figure 13: More results on CelebA-HQ.



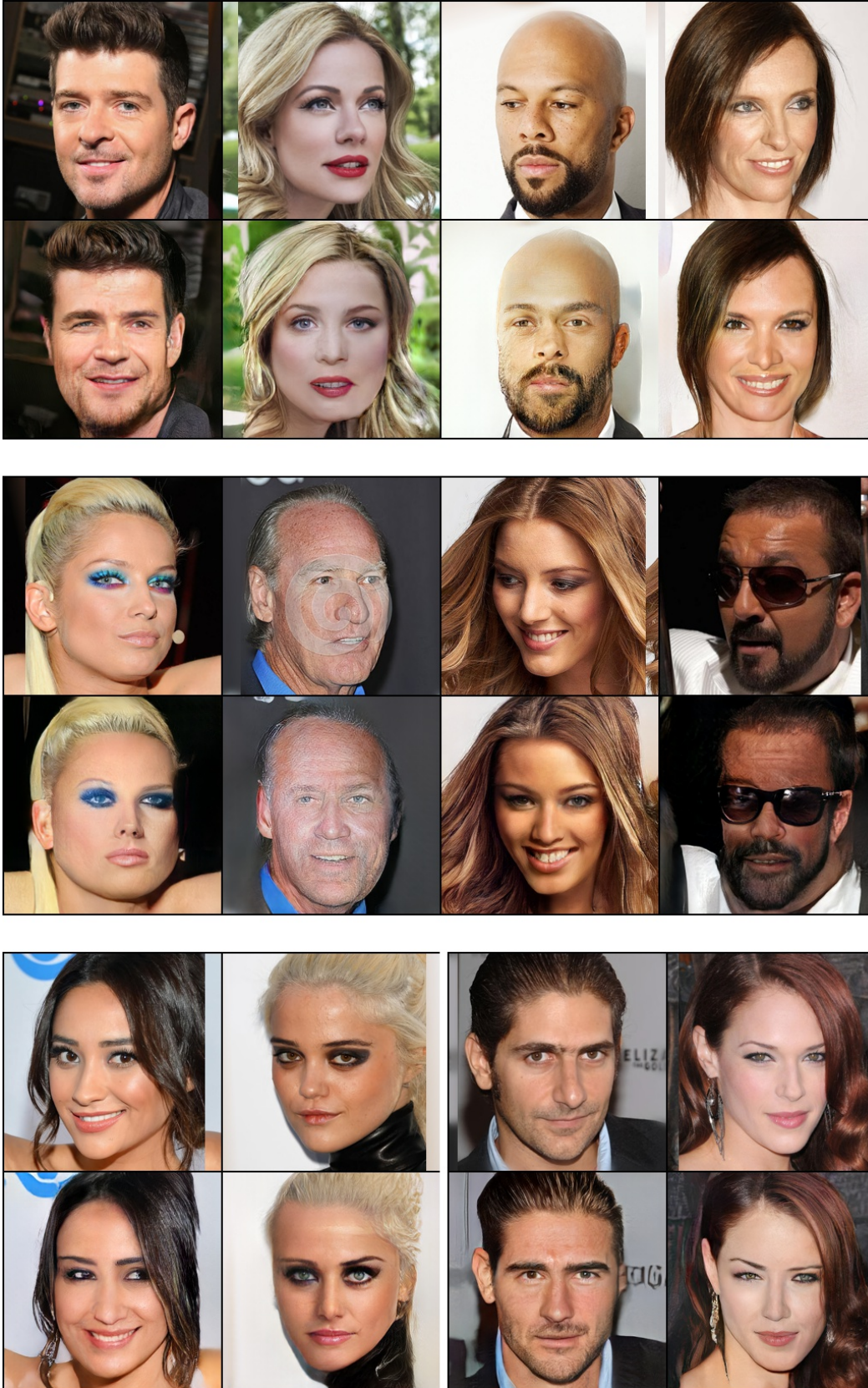


Figure 14: More results on CelebA-HQ.